A revised global estimate of dissolved iron fluxes from marine sediments

A. W. Dale, L. Nickelsen, F. Scholz, C. Hensen, A. Oschlies, K. Wallmann

GEOMAR Helmholtz Centre for Ocean Research Kiel, Kiel, Germany

Contents of this file

Introduction

This Supplement describes the numerical model used to simulate the biogeochemical dynamics in marine sediments.

Text S1.

A numerical reaction-transport model for quantifying benthic fluxes

This text describes the numerical model used to simulate the biogeochemical dynamics in marine sediments. Section 1.1 describes the basic model architecture including the transport processes; Section 1.2 describes the biogeochemical reaction network; Section 1.3 presents the POC degradation kinetics; Section 1.4 presents details on the boundary conditions and model solution. The model has been published several times previously for specific steady and non-steady state applications (Dale et al., 2010; 2011; 2012; 2013).

1.1. Numerical framework

A vertically-resolved 1-D reaction-transport model (RTM) was used to simulate the distribution of the chemical species listed in Table S1 in the upper 30 cm of sediment.

The model includes the most important transport pathways of solid particles and interstitial fluids in sedimentary environments and simultaneously accounts for production and consumption of chemical species by biogeochemical reactions. Mathematically, these processes can be summarized as the following mass-conservation equations (Berner, 1980; Boudreau, 1997):

$$\varphi \frac{\partial C_a(z,t)}{\partial t}$$
$$= \frac{\partial}{\partial z}\left(\varphi D \frac{\partial C_a(z,t)}{\partial z}\right) - \frac{\partial \varphi v_a C_a(z,t)}{\partial z} + \alpha\varphi\big(C_a(0,t) - C_a(z,t)\big) + \Sigma\varphi R(z,t) \qquad (1a)$$

$$(1-\varphi) \frac{\partial C_s(z,t)}{\partial t}$$
$$= \frac{\partial}{\partial z}\left((1-\varphi)D_b \frac{\partial C_s(z,t)}{\partial z}\right) - \frac{\partial (1-\varphi)v_s C_s(z,t)}{\partial z} + \Sigma(1-\varphi)R(z,t) \qquad (1b)$$

where $C_a(z,t)$ and $C_s(z,t)$ are the concentrations of solutes in mmol cm^{-3} (of pore water) and particulate species in weight percent of dry sediment (%), respectively, z (cm) denotes depth in the sediment, t (yr) is time, φ is porosity, v_a (cm yr^{-1}) and v_s (cm yr^{-1}) are the burial velocities of porewater and solids, respectively, D (cm^2 yr^{-1}) is the sedimentary molecular diffusion coefficient, D_b (cm^2 yr^{-1}) is the bioturbation coefficient representing sediment mixing by animals, α (y^{-1}) is the bioirrigation coefficient for solutes and $C_a(0,t)$ is the solute concentration at the sediment-water interface. ΣR is the sum of the rate of change of concentration due to biogeochemical reactions. Constitutive equations describing the depth dependency of φ, D, v_s, v_a, D_b, and α are provided in Table S2. Corresponding model parameters are listed in Table S3 and Table 2 in the main text.

Porosity describes the volume of porewater relative to the volume of total sediment. Similarly, the solid components of the sediment occupy a volume fraction equal to 1-φ. Porosity generally decreases with depth in the sediment due to steady state compaction (Berner, 1980). The function for porosity used in the model is based on the widely observed exponential decrease with sediment depth (Berner, 1980).

Molecular diffusion coefficients for solutes in seawater, D_W (cm^2 y^{-1}), were calculated using data provided by Boudreau (1997) and Schulz (2000) for the relevant temperature and salinity. In situ diffusion coefficients of each dissolved species, D, were further corrected for tortuosity (Boudreau, 1997). This phenomenon accounts for the longer path length for solutes to diffuse around particles in sediments.

Relative to the sea floor, both solids and solutes are advected downwards due to accumulation of new sediment at the surface. However, as a result of compaction, pore fluids are expelled upwards relative to the sediment particles. Equations for the burial velocity of solutes and solids (Table S2) were taken from Berner (1980).

Bioturbation, the stirring of the sediment by animals, is assumed not to affect porosity gradients (i.e. intraphase mixing; Boudreau, 1986). Bioturbation was formulated as a diffusive process where the mixing rate at the sediment surface is defined by the coefficient $D_b(0)$ (cm^2 yr^{-1}). With increasing sediment depth, bioturbation becomes less intense, reflecting the overall decrease in metazoan abundance. This change in bioturbation intensity with sediment is described using a Gaussian-type function, where the parameter z_{bt} (cm) is the bioturbation halving depth (Boudreau, 1996).

Burrowing macrofauna that build and live inside tube-like structures ventilate their burrows by pumping seawater through and around their bodies. This process, termed bioirrigation, leads to a rapid exchange of porewater and seawater and reduced concentration gradients of solutes between the sediment and overlying water column (Aller and Aller, 1998). Bioirrigation, like bioturbation, tends to be highest on the continental margins where food availability is higher (Glud et al., 1994; Meile and van Cappellen, 2003). Bioirrigation was described as a non-local 1-D mixing process whose rate depends on the difference in solute concentration between the water column and sediment (Table S2). Irrigation intensity at the sediment surface is defined by the parameter $\alpha(0)$ (yr^{-1}). Irrigation decreases with sediment depth following a simple exponential function with an attenuation coefficient, z_{bio} (cm) (Martin and Banta, 1992).

1.2. Biogeochemical reactions

The set of coupled biogeochemical reactions included in the model (Table S4) is similar to those published previously (e.g. Dhakar and Burdige, 1996; Van Cappellen and Wang, 1996; Berg et al., 2003). In this study, 12 solutes and 13 solid species were considered (Table S1). The cycling of chemical elements is ultimately driven by the mineralization of organic matter (OM) by microorganisms using specific electron acceptors (e.g. O_2, NO_2^-, NO_3^-, Mn^{IV}, Fe^{III}, SO_4^{2-}). OM is chemically defined as $CN_{rNC}P_{rPC}$ with a carbon oxidation state of zero and where r_{NC} and r_{PC} are the (Redfield) atomic ratios of particulate organic nitrogen and phosphorus to carbon in this material. Electron acceptors are mainly delivered to the sediment from the overlying water column but may also, with the exception of O_2 in the absence of benthic photosynthesis, be produced in situ by re-oxidation of their reduced forms. The order in which the electron acceptors are consumed broadly reflects the Gibbs energy yield per mole of carbon respired (Froelich et al., 1979). Accordingly, OM is first mineralized by aerobic respiration, followed by denitrification, manganese oxide reduction, iron oxide reduction, sulfate reduction and methanogenesis (Table S5). This sequence is maintained in the model through the use of dimensionless limitation terms based on the availability of electron acceptors (e.g. Berner, 1980; Boudreau, 1997). In contrast to the previous models listed above, ours includes nitrite as an additional electron acceptor. This step was taken since it provides a more realistic description of the N cycle (Bohlen et al., 2011). OM degradation kinetics is described separately in the following section.

The metabolic (dissolved) end products of OM degradation are free to be exported from the sediment or take part in secondary redox reactions. These reactions largely follow Van Cappellen and Wang (1996), Berg et al. (2003) and Dale et al. (2009). In keeping with common practice, the rates of these processes are generally described as first- or second-order rates expressions (Table S5). Kinetic constants were also taken from those studies (Table S3). Main differences between our model and previous versions mainly relate to N and Fe cycling. Firstly, our model considers a more complete N cycle, including dissimilatory nitrate reduction to ammonium (DNRA, R_8) and anaerobic ammonium oxidation (anammox, R_9). DNRA mainly occurs in sediments underlying near-anoxic bottom water (e.g. Otte et al., 1999). In this study, we set this reaction to zero in the standard shelf and slope model simulations since these regions comprise much less than 1 % of the continental margin area (Bohlen et al., 2012). Nitrate

can be produced and consumed by several reactions including denitrification (R_2, R_3) and nitrification (R_{10}, R_{11}) and anammox. Nitrate can also be denitrified by reaction with ferrous iron (R_{14}) (Dhakar and Burdige, 1996). Kinetic constants for the N cycle were mainly taken the empirical model study of Bohlen et al. (2011).

The reactivity of iron (oxyhydr)oxides (hereafter Fe oxides) was defined according to the widely-employed classification based on wet chemical extraction methods (Canfield et al., 1992; Raiswell and Canfield, 1998; Poulton et al., 2004). These studies have shown that reactive Fe oxides can be broadly defined as being highly reactive (Fe_{HR}), moderately reactive (Fe_{MR}) or poorly reactive (Fe_{PR}). Fe_{HR} has a half-life of < 1 yr and represents iron contained within amorphous and reactive crystalline oxides (ferrihydrite, goethite, lepidocrocite and hematite), pyrite and acid volatile sulfides, plus a small fraction of iron in reactive silicates (Canfield et al., 1992; Raiswell and Canfield, 1998). Fe_{PR} has a half-life of at least 10^5 yr and represents iron released from a wide range of reactive silicates and magnetite. Fe_{MR} comprises all the iron with a reactivity intermediate between Fe_{HR} and Fe_{PR} (i.e. magnetite and reactive silicates) with a half life of 10^2 yr. An additional detrital iron fraction, representing Fe bound within sheet silicates (Fe_U), is essentially unreactive on early diagenetic time scales and constitutes about half of all sedimentary iron underlying oxic waters (Poulton and Raiswell, 2002). The model simulates all four of these fractions, defined chemically as $Fe(OH)_3$. Similarly, two pools of manganese oxide were considered: Mn_{HR} and Mn_{MR} (Berg et al., 2003).

Particulate Fe was added to the sediment by deposition from the water column. Fe_{HR} can be also produced authigenically via the aerobic oxidation of ferrous iron that diffuses into the surface oxidized zone from the underlying anaerobic layers. This process is the most efficient geochemical barrier to ferrous iron release from the sediment (McManus et al., 1997; Berg et al., 2003). The rate was parameterized using a linear dependency on Fe^{2+} and O_2 concentrations (Millero et al., 1987). We also allow oxidation of Fe^{2+} to occur using Mn(IV) and, as mentioned, NO_3^-, as the electron acceptor. All fractions (except Fe_U) can be reduced by porewater sulfide according to the reaction kinetics proposed by Poulton et al. (2004), leading to production of dissolved ferrous iron and particulate elemental sulfur, S^0. The rate of iron reduction is linearly dependent on the iron concentration and shows a square root dependence on sulfide concentration (Table S5). The rate constants for these reactions were defined based on the half-lives listed above assuming a 1 mM sulfide concentration (see also Poulton et al. (2004)). This equates to rate constants which are broadly definable as 100, 0.1 and 0.0003 $L^{0.5}$ $mol^{-0.5}$ yr^{-1} for Fe_{HR}, Fe_{MR} and Fe_{PR}, respectively. Previous approaches considered only the total iron concentration with a single bulk reactivity (Van Cappellen and Wang, 1996; Berg et al., 2003). Fe_{HR} has an additional sink due to dissimilatory iron reduction (DIR), whereas the other phases are too crystalline (unreactive) to be of benefit to iron reducing bacteria (Weber, et al., 2006). Fe_{HR} also slowly undergoes preservation or ageing into more crystallization phases such as goethite and hematite (Lijklema, 1980; Cornell and Schwertmann, 1996). This is conceptualized in the model by transformation to Fe_{MR}. In a study on the Arctic shelf, the ageing half-life of Fe_{HR} was calculated to be 0.7 years (Berg et al., 2003). We use the same proportionality constant in our model, whilst noting that the ageing process is one of least well-constrained aspects of our model. Ageing of Mn_{HR} to Mn_{MR} is treated analogously. The iron module also includes iron mono-sulfide precipitation (R_{19}) and pyrite precipitation (R_{20}, R_{21}). The latter can occur via the H_2S

pathway (Berzelius reaction) or by reaction with S^0 (Bunsen reaction) (Rickard and Luther, 2007). Finally, molecular hydrogen produced by pyritization can be oxidized by all electron acceptors (EA), producing electron donors (ED, R_{22}). Including a sink for H_2 conserves electrons in the sediment (Meysman and Middelburg, 2005).

Iron carbonate (siderite) was not considered in the model since siderite precipitation is inhibited by low levels of sulfide (Haese, 2000). However, the precipitation of siderite is strongly dependent on the Eh-pH conditions, and co-precipitation of siderite and pyrite may occur simultaneously in micro-environments within the sediment matrix (Bell et al., 1987). Since our model does not resolve pH explicitly, and considering that siderite appears to be quantitatively unimportant in near-surface sediments in both marginal (Rajendran et al., 1992) and deep sea sediments environments (Ellwood et al., 1988), we have chosen to ignore siderite dynamics in the model.

1.3. Organic carbon degradation

1.3.1. Background

Mineralization of OM is arguably the most important process to parameterize correctly since the rate and depth at which it takes place will determine the proportion in which the electron acceptors are consumed and the rate at which reducing equivalents are produced. For instance, highly reactive OM with half life of days to weeks will tend to be respired by oxygen and nitrate in the upper oxidized layer. The consumption of electron acceptors will, therefore, be largely controlled by the amount and reactivity of organic matter at any given depth in the sediment, which is in turn controlled by the rate of sediment burial and mixing. A realistic simulation of the redox structure of the sediment thus requires sound definition of the degradation kinetics.

OM can be envisaged as a complex mixture of high molecular weight compounds. Because these compounds cannot be taken up by microbes directly, extracellular hydrolysis and fermentation is required to produce smaller, monomeric molecules such as sugars, amino acids and hydrogen (Megonigal et al., 2004). These steps are normally considered to determine the rate at which OM decay takes place (Arnosti, 2004) although thermodynamic limitations may also be important (LaRowe and Van Cappellen, 2011). Most model applications typically assume that bulk organic matter is present in discrete pools (often referred to as '*G*' fractions), each characterized by its own reactivity or first-order rate constant, k, with units of inverse time (e.g. Jørgensen, 1978; Westrich and Berner, 1984). In many cases, OM degradation has been described quantitatively using 1 to 3 reactive fractions (i.e. 'multi-*G*' model, reviewed by Regnier et al. (2011) and Arndt et al., 2013)). However, the degradation of OM in the upper few mm where reaction rates are highest are often poorly described due to a lack of sufficiently resolved data to constrain the highly reactive fractions.

An alternative approach to the multi-*G* model is based on the reactive continuum theory of OM degradation kinetics (Boudreau and Ruddick, 1991). Here, OM (hereafter POC to make carbon the point of reference) is assumed to be composed of an infinite number of fractions each with its own k. The apparent reactivity of POC is defined by the changing composition of the mass with time. Assuming first-order decay of each fraction,

the bulk POC sample is initially (at $t = 0$) distributed over k according to the Gamma distribution (Boudreau and Ruddick, 1991):

$$g(k,0) = \frac{g_0 \cdot k^{v-1} \cdot e^{-a \cdot k}}{\Gamma(v)} \qquad (2)$$

where $g(k,0)$ is a probability density function (PDF) which determines the concentration of G described by a decay constant k at time zero, or more precisely the G concentration having a reactivity between k and $k + dk$ where dk is an infinitesimal increment in k. In Eq. (2), Γ is the Gamma function, a (yr) is the average live time of the more reactive components of the mixture, and v is a dimensionless parameter determining the shape of the distribution near $k = 0$. Low values of v indicate that the bulk organic matter is dominated by refractory components clustered near $k = 0$, whereas higher values correspond to a more even distribution of reactive types. Similarly, organic matter characterized by low a will be rapidly degraded and vice-versa.

The Gamma function satisfies the following relation:

$$\Gamma(v) = \int_0^\infty x^{v-1} \cdot e^{-x} dx \qquad (3)$$

while g_0 is defined as (Boudreau and Ruddick, 1991):

$$g_0 = G(0) \cdot a^v \qquad (4)$$

where $G(0)$ is the initial total concentration POC at $t = 0$. In a closed system (i.e. a non-mixed sediment), the initial Gamma distribution corresponds to a very simple $G(t)$ function (Boudreau and Ruddick, 1991):

$$G(t) = \frac{g_0}{(a+t)^v} = G(0) \cdot \left(\frac{a}{a+t}\right)^v \qquad (5)$$

where $G(0)$ is the initial concentration of total POC and $G(t)$ defines the decrease of total POC over time (t). The POC degradation rate is defined as differential of $G(t)$ over time:

$$\frac{dG(t)}{dt} = -\frac{v \cdot g_0}{(a+t)^{v+1}} = -\frac{v \cdot G(0) \cdot a^v}{(a+t)^{v+1}} = -v \cdot (a+t)^{-1} \cdot G(t) \qquad (6)$$

1.3.2. Approximation of reactive continuum model using multi-G kinetics

Reactive continuum-type models are useful to describe the down-core change in organic matter reactivity below the bioturbated zone but are very difficult to apply for bioturbated surface sediments since the age and reactivity of organic matter within the bioturbated zone are only poorly constrained (Boudreau and Ruddick, 1991; Meile and Van Cappellen, 2005; Middelburg, 1989; Rothman and Forney, 2007). Ages of reactive

tracers within the bioturbated zone depend not only on burial velocity and bioturbation rate but also on the reactivity of the tracer (Meile and Van Cappellen, 2005). So far, POC ages in bioturbated sediments have only been determined assuming simple first-order degradation kinetics (Meile and Van Cappellen, 2005). POC ages determined using reactive continuum models are virtually unknown. Furthermore, reactive POC fractions may be preferentially taken up and displaced by benthic macro-fauna within the bioturbated layer (Smith et al., 1993).

We used a multi-G model to simulate the continuum model in bioturbated sediments where POC was represented by a finite number of different fractions each having their own first-order decay constant, k. The multi-G model was constructed applying the Gamma distribution. For $a > 0$ and $k > 0$:

$$f(k,0) = \frac{a^{v} \cdot k^{v-1} \cdot e^{-a \cdot k}}{\Gamma(v)} \tag{7}$$

where $f(k,0)$ is a PDF which determines the fraction of POC having a reactivity of k at time zero. The corresponding cumulative distribution function (CDF) is defined as:

$$F(k,0) = \frac{\Gamma(v,0,a \cdot k)}{\Gamma(v)} = \frac{\int_{0}^{a \cdot k} x^{v-1} \cdot e^{-x} dx}{\int_{0}^{\infty} x^{v-1} \cdot e^{-x} dx} \tag{8}$$

where $F(k,0)$ gives the fraction of total POC having a reactivity $\leq k$ at $t = 0$. A 14-G model was constructed by separating POC into 14 different species. The fraction of total POC having the kinetic constant $k_i = 10^{-i+1/2}$ yr^{-1} for given values of a and v was calculated as:

$$F_i(k_i,0) = \frac{\Gamma(v,0,a \cdot k_{i+1}) - \Gamma(v,0,a \cdot k_i)}{\Gamma(v)} = \frac{\int_{0}^{a \cdot k_{i+1}} x^{v-1} \cdot e^{-x} dx - \int_{0}^{a \cdot k_i} x^{v-1} \cdot e^{-x} dx}{\int_{0}^{\infty} x^{v-1} \cdot e^{-x} dx} \tag{9}$$

for i = -10 to +1.

The low-reactivity fraction with a kinetic constant $k \leq 10^{-10}$ yr^{-1} was calculated from the CDF as:

$$F_i(10^{-10},0) = \int_{0}^{a \cdot 10^{-10}} x^{v-1} \cdot e^{-x} dx \tag{10}$$

The high reactivity fraction with a kinetic constant $k \geq 100$ yr^{-1} was calculated as:

$$F_i(100,0) = \frac{\int_{0}^{a \cdot \infty} x^{v-1} \cdot e^{-x} dx - \int_{0}^{a \cdot 100} x^{v-1} \cdot e^{-x} dx}{\int_{0}^{\infty} x^{v-1} \cdot e^{-x} dx} \tag{11}$$

Values of a (3×10^{-4} yr^{-1}) and v (0.125) were calculated by Boudreau et al. (2008) using data from an experiment where fresh phytoplankton was degraded over a 2 yr period (Westrich and Berner, 1984). The POC fractions and kinetic constants that define these Gamma distribution values are:

POC$_1$:	$k_1 = 1\times10^{-10}$ yr^{-1},	$F_1 = 0.021746$
POC$_2$:	$k_2 = 3.16\times10^{-10}$ yr^{-1},	$F_2 = 0.00725275$
POC$_3$:	$k_3 = 3.16\times10^{-9}$ yr^{-1},	$F_3 = 0.0096717$
POC$_4$:	$k_4 = 3.16\times10^{-8}$ yr^{-1},	$F_4 = 0.0128974$
POC$_5$:	$k_5 = 3.16\times10^{-7}$ yr^{-1},	$F_5 = 0.017199$
POC$_6$:	$k_6 = 3.16\times10^{-6}$ yr^{-1},	$F_6 = 0.0229352$
POC$_7$:	$k_7 = 3.16\times10^{-5}$ yr^{-1},	$F_7 = 0.0305846$
POC$_8$:	$k_8 = 3.16\times10^{-4}$ yr^{-1},	$F_8 = 0.0407852$
POC$_9$:	$k_9 = 3.16\times10^{-3}$ yr^{-1},	$F_9 = 0.0543879$
POC$_{10}$:	$k_{10} = 0.0316$ yr^{-1},	$F_{10} = 0.0725265$
POC$_{11}$:	$k_{11} = 0.316$ yr^{-1},	$F_{11} = 0.0967046$
POC$_{12}$:	$k_{12} = 3.16$ yr^{-1},	$F_{12} = 0.12881$
POC$_{13}$:	$k_{13} = 31.6$ yr^{-1},	$F_{13} = 0.169822$
POC$_{14}$:	$k_{14} = 100$ yr^{-1},	$F_{14} = 0.314677$

where the fractions F_i add up to unity.

The multi-G model was tested in a batch set-up to compare the model performance with the analytical solution of the continuum model for the phytoplankton degradation experiment. The following system of initial conditions and ordinary differential equations defines the multi-G model in a batch set-up (no transport):

$$\sum_{i=1}^{14}\left(POC_i(0) = F_i \cdot POC_T(0)\right) \qquad \sum_{i=1}^{14}\left(\frac{dPOC_i}{dt} = -k_i \cdot POC_i\right) \qquad (12)$$

The analytical solution results as:

$$POC_T = \sum_{i=1}^{14}\left(F_i \cdot POC_T(0) \cdot e^{-k_i \cdot t}\right) \qquad (13)$$

where POC_T is the total POC concentration. This solution was tested against the analytical solution of the continuum model:

$$POC_T = POC_T(0) \cdot \left(\frac{a}{a+t}\right)^v \qquad (14)$$

with $a = 3\times10^{-4}$ yr^{-1}, $v = 0.125$, and $POC_T(0) = 13.3$ wt-%. Figure S1 shows that the results of the multi-G model (blue line) are consistent with the continuum model (red line). Only at $t < 0.05$ yr, a significant deviation occurs since the multi-G model does not resolve changes in reactivity for $k > 20$ yr^{-1}. The multi-G model based on 14 discrete

fractions is, however, a good approximation of the continuum model for the time period relevant for most bioturbated sediments (0.05 – 10 000 yr).

The 14-*G* model was implemented into the differential equation (Eq. 1) after defining values of *a* and *υ*. We used the above values of *a* and *υ* applicable to fresh phytoplankton in the simulations.

1.4. Model boundary conditions and solution

Robin type (constant flux) conditions were used for the solid species at the upper boundary (see Table S1 and Table 2 in main text). For solutes, a diffusive boundary layer of 0.04 cm thickness was assumed and implemented as described by Boudreau (1996). Dirichlet type (fixed concentration) boundary conditions were used for solutes in seawater, corresponding to mean oceanic values. At the lower boundary, all species were prescribed with a zero flux (Neumann) boundary condition. To solve the model, the continuous spatial derivatives in Eq. (1) were replaced with finite differences considering an unevenly spaced grid of 100 layers (Boudreau, 1997). The resulting set of ordinary differential equations was solved using the NDSolve algorithm in MATHEMATICA 7.0 using the method of lines (Boudreau, 1996). A high spatial resolution of 0.03 cm was used at the surface to minimize numerical errors in the layers where reaction rates are highest. At the base of the sediment, the grid thickness increased to 1.9 cm. A centered finite difference scheme was used for dissolved species and solid species within the bioturbated zone. An upward scheme was applied for the transport of solids below this depth to avoid numerical instabilities (Boudreau, 1996). The model was run using a long simulation time (10^4 yr) until steady-state conditions were achieved. Mass conservation for each species was checked by comparing depth-integrated reaction rates with fluxes across the model boundaries.

References

Aller, R. C., Aller, J. Y. (1998) The effect of biogenic irrigation intensity and solute exchange on diagenetic reaction rates in marine sediments. *J. Mar. Res.,* 56, 905-936.

Arndt, S., Jørgensen, B. B., LaRowe, D. E., Middelburg, J. J., Pancost, R. D., Regnier, P. (2013) Quantifying the degradation of organic matter in marine sediments: A review and synthesis. *Earth-Sci. Rev.,* 123, 53-86.

Arnosti, C. (2004) Speed bumps and barricades in the carbon cycle: substrate structural effects on carbon cycling. *Mar. Chem.,* 92, 263-273.

Bell, P. E., Mills, A. L., Herman, J. S. (1987) Biogeochemical conditions favoring magnetite formation during anaerobic iron reduction. *App. Environ. Microbiol.,* 53, 2610-2616.

Berg, P., Rysgaard, S., Thamdrup, B. (2003) Dynamic modeling of early diagenesis and nutrient cycling. A case study in an Arctic marine sediment. *Am. J. Sci.,* 303, 905-955.

Berner, R. A. (1980) Early Diagenesis: A Theoretical Approach, Princeton University Press, Princeton, 241 pp.

Bohlen, L., Dale, A. W., Sommer, S., Mosch, T., Hensen, C., Noffke, A., Scholz, F., Wallmann, K. (2011) Benthic nitrogen cycling traversing the Peruvian oxygen minimum zone. *Geochim. Cosmochim. Acta,* 75, 6094-6111.

Bohlen, L., Dale, A. W., Wallmann, K. (2012) Simple transfer functions for calculating benthic fixed nitrogen losses and C:N:P regeneration ratios in global biogeochemical models. *Glob. Biogeochem. Cy.,* 26, GB3029, doi:10.1029/2011GB004198.

Boudreau, B. P. (1986) Mathematics of tracer mixing in sediments; I, Spatially-dependent, diffusive mixing. *Am. J. Sci.,* 286, 161-198.

Boudreau, B. P. (1996) A method-of-lines code for carbon and nutrient diagenesis in aquatic sediments. *Comput. Geosci.,* 22, 479-496.

Boudreau, B. P. (1997) Diagenetic Models and Their Implementation: Modelling Transport and Reactions in Aquatic Sediments, Springer-Verlag, Berlin, 414 pp.

Boudreau, B. P., Ruddick, B. R. (1991) On a reactive continuum representation of organic matter diagenesis. *Am. J. Sci.,* 291, 507-538.

Canfield, D. E., Raiswell, R., Bottrell, S. (1992) The reactivity of sedimentary iron minerals toward sulfide. *Am. J. Sci.,* 292, 659-683.

Cornell, R. M., Schwertmann, U. (1996) The Iron Oxides: Structure, Properties, Reactions, Occurrences and Uses, Wiley-VCH, Darmstadt, Germany, 703 pp.

Dale, A. W., Brüchert, V., Alperin, M., Regnier, P. (2009) An integrated sulfur isotope model for Namibian shelf sediments. *Geochim. Cosmochim. Acta,* 73, 1924-1944.

Dale, A. W., Sommer, S., Haeckel, M., Wallmann, K., Linke, P., Wegener, G., Pfannkuche, O. (2010) Pathways and regulation of carbon, sulfur and energy transfer in marine sediments overlying methane gas hydrates on the Opouawe Bank (New Zealand). *Geochim. Cosmochim. Acta,* 74, 5763-5784.

Dale, A. W., Sommer, S., Bohlen, L., Treude, T., Bertics, V. J., Bange, H. W., Pfannkuche, O., Schorp, T., Mattsdotter, M., Wallmann, K. (2011) Rates and regulation of nitrogen cycling in seasonally hypoxic sediments during winter (Boknis Eck, SW Baltic Sea): sensitivity to environmental variables. *Estuar. Coast. Shelf Sci.,* 95, 14-28.

Dale, A. W., Meyers, S. R., Aguilera, D. R., Arndt, S., Wallmann, K. (2012) Controls on carbon and molybdenum accumulation rates in Cretaceous marine sediments from the Cenomanian-Turonian interval including Oceanic Anoxic Event 2. *Chem. Geol.,* 324-325, doi:10.1016/j.chemgeo.2011.10.004.

Dale, A. W., Bertics, V. J., Treude, T., Sommer, S., Wallmann, K. (2013) Modeling benthic–pelagic nutrient exchange processes and porewater distributions in a seasonally hypoxic sediment: evidence for massive phosphate release by *Beggiatoa*? *Biogeosciences,* 10, 629-651, doi:10.5194/bg-10-629-2013.

Dhakar, S. P., Burdige, D. J. (1996) A coupled, non-linear, steady-state model for early diagenetic processes in pelagic sediments. *Am. J. Sci.,* 296, 296-330.

Ellwood, B. B., Chrzanowski, T. H., Frantisek Hrouda, F., Long, G. J., Buhl, M. L. (1988) Siderite formation in anoxic deep-sea sediments: A synergetic bacteria controlled process with improtant implications in paleomagnetism. *Geology,* 16, 980-982.

Froelich, P. N., Klinkhammer, G. P., Bender, M. L., Luedtke, N. A., Heath, G. R., Cullen, D., Dauphin, P. (1979) Early oxidation of organic matter in pelagic sediments of the eastern equatorial Atlantic: suboxic diagenesis. *Geochim. Cosmochim. Acta,* 43, 1075-1090.

Glasby, G. P. (2006) Manganese: Predominant role of nodules and crusts, in Marine Geochemistry 2nd edition, edited by H. D. Schulz and M. Zabel, pp 391-427, Springer-Verlag, Berlin.

Glud, R. N., Gundersen, J. K., Jorgensen, B. B., Revsbech, N. P., Schulz, H. D. (1994) Diffusive and total oxygen uptake of deep-sea sediments in the eastern South Atlantic Ocean: in situ and laboratory measurements. *Deep-Sea Res.,* II 41, 1767-1788.

Haese, R. R. (2000) The reactivity of iron, in Marine Geochemistry, edited by H. D. Schulz and M. Zabel, pp 233-261, Springer-Verlag, Berlin.

Jørgensen, B. B. (1978) A comparison of methods for the quantification of bacterial sulfate reduction in coastal marine sediments. II Calculation from mathematical models. *Geomicrobiol. J.,* 1, 29-47.

LaRowe, D. E., Van Cappellen, P. (2011) Degradation of natural organic matter: A thermodynamic analysis. *Geochim. Cosmochim. Acta* 75, 2030-2042.

Lijklema, L. (1980) Interaction of orthophosphate with iron(III) and aluminum hydroxides. *Environ. Sci. Technol.,* 14, 537-541. 1980.

Linke, P., Wallmann, K., Suess, E., Hensen, C., Rehder, G. (2005) In situ benthic fluxes from an intermittently active mud volcano at the Costa Rica convergent margin. *Earth Planet. Sci. Lett.* 235, 79-95.

Martin, W. R., Banta, G. T. (1992) The measurement of sediment irrigation rates: A comparison of the Br- tracer and 222Rn/226Ra disequilibrium techniques. *J. Mar. Res.,* 50, 125-154.

McManus, J., Berelson, W. M., Coale, K. H., Johnson, K. S., Kilgore, T. E. (1997) Phosphorus regeneration in continental margin sediments. *Geochim. Cosmochim. Acta,* 61, 2891-2907.

Megonigal, J.P., M.E. Hines, and P.T. Visscher. (2004) Anaerobic metabolism: Linkages to trace gases and aerobic processes, Biogeochemistry, edited by W. H. Schlesinger, pp 317-424, Elsevier-Pergamon, Oxford, UK.

Meile, C., Van Cappellen, P. (2003) Global estimates of enhanced solute transport in marine sediments. *Limnol. Oceanogr.,* 48, 777-786.

Meile, C., Van Cappellen, P. (2005) Particle age distributions and O_2 exposure times: Timescales in bioturbated sediments. *Glob. Biogeochem. Cy.,* 19, GB3013, doi:10.1029/2004GB002371.

Meile, C., Berg, P., Van Cappellen, P., Tuncay, K. (2005) Solute-specific pore water irrigation: Implications for chemical cycling in early diagenesis. *J. Mar. Res.,* 64, 601-621.

Meysman, F. J. R., Middelburg, J. J. (2005) Acid-volatile sulfide (AVS) — A comment. *Mar. Chem.,* 97, 202-212.

Middelburg, J. J. (1989) A simple rate model for organic matter decomposition in marine sediments. *Geochim. Cosmochim. Acta,* 53, 1577-1581.

Millero, F. J., Sotolongo, S., Izaguirre, M. (1987) The oxidation kinetics of Fe(II) in seawater. *Geochim. Cosmochim. Acta,* 51, 793-801.

Otte, S., Kuenen, J. G., Nielsen, L. P., Paerl, H. W., Zopfi, J., Schulz, H. N., Teske, A., Strotmann, B., Gallardo, V. A., Jørgensen, B. B. (1999) Nitrogen, carbon, and sulfur metabolism in natural Thioploca samples. *App. Environ. Microbiol.,* 65, 3148-3157.

Raiswell, R., Canfield, D. E. (1998) Sources of iron for pyrite formation in marine sediments. *Am. J. Sci.,* 298, 219-245.

Poulton, S. W., Raiswell, R. (2002) The low-temperature geochemical cycle of iron: From continental fluxes to marine sediment deposition. *Am. J. Sci.,* 302, 774-805.

Poulton, S. W., Krom, M. D., Raiswell, R. (2004) A revised scheme for the reactivity of iron (oxyhydr)oxide minerals towards dissolved sulfide. *Geochim. Cosmochim. Acta,* 68, 3703-3715.

Rajendran, A., Dileep Kumar, M., Bakker, J. F. (1992) Control of manganese and iron in Skagerrak sediments (northeastern North Sea). *Chem. Geol.,* 98, 111-129.

Redfield, A. C., Ketchum, B. H., Richards, F. A. (1963). The influence of organisms on the composition of seawater, in The Sea, edited by M. N. Hill, pp 26-77, Interscience, New York.

Regnier, P., Dale, A. W., Arndt, S., LaRowe, D. E., Mogollón, J. M., Van Cappellen, P. (2011) Quantitative analysis of anaerobic oxidation of methane (AOM) in marine sediments: A modelling perspective. *Earth-Sci. Rev.,* 106, 105-130.

Rickard, D., Luther III, G. W. (2007) Chemistry of iron sulfides. *Chem. Rev.,* 107, 514-562.

Rothman, D. H., Forney, D. C. (2007) Physical model for the decay and preservation of marine organic carbon. *Science,* 316, 1325-1328.

Schulz, H. D. (2000) Conceptual models and computer models, in Marine Geochemistry, edited by H. D. Schulz and M. Zabel, pp 417-442, Springer-Verlag, Berlin.

Smith, C. R., Pope, R. H., DeMaster, D. J., Magaard, L. (1993) Age-dependent mixing of deep-sea sediments. *Geochim. Cosmochim. Acta,* 57, 1473-1488.

Van Cappellen, P., Wang, Y. (1996) Cycling of iron and manganese in surface sediments: a general theory for the coupled transport and reaction of carbon, oxygen, nitrogen, sulfur, iron, and manganese. *Am. J. Sci.,* 296, 197-243.

Weber, K. A., Achenbach, L. A., Coates, J. D. (2006) Microorganisms pumping iron: anaerobic microbial iron oxidation and reduction. *Nat. Rev. Microbiol.,* 4, 752-764.

Westrich, J. T., Berner, R. A. (1984). The role of sedimentary organic matter in bacterial sulfate reduction: the G-model tested. *Limnol. Oceanogr.,* 29, 236-249.
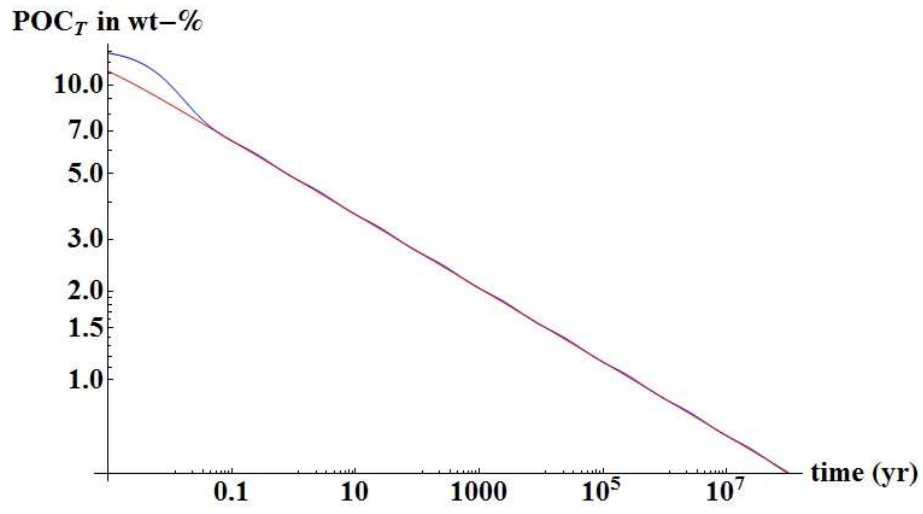
Figure S1. Comparison of analytical solutions of the 14-G model (blue line) and the continuum model (red line).

Variable	Value [a]
Solutes	
Oxygen (C_{O2}) [b]	Variable (see main text)
Nitrate (C_{NO3})	35×10^{-6}
Nitrite (C_{NO2})	0
Sulfate (C_{SO4})	28×10^{-3}
Ferrous iron (C_{Fe})	0
Manganese (C_{Mn})	0
Ammonium (C_{NH4})	1×10^{-6}
Total phosphate (C_{PO4})	2×10^{-6}
Total inorganic carbon (C_{TCO2})	2×10^{-3}
Total sulfide (C_{H2S})	0
Methane (C_{CH4})	0
Hydrogen (C_{H2})	0
Solids	
Organic carbon (F_{POC})	Variable (see main text)
Organic nitrogen (F_{POC})	$F_{POC} \cdot r_{NC}$
Organic phosphorus (F_{POP})	$F_{POC} \cdot r_{PC}$
Adsorbed ammonium (F_{NH4ads})	0
Total Fe oxide (F_{FeT})	Variable (see main text)
Highly reactive Fe oxide (F_{FeHR})	$F_{FeT} \times {}^1/_6$
Moderately reactive Fe oxide (F_{FeMR})	$F_{FeT} \times {}^1/_6$
Poorly reactive Fe oxide (F_{FePR})	$F_{FeT} \times {}^1/_6$
Unreactive Fe oxide (F_{FeU})	$F_{FeT} \times {}^1/_2$
Total Mn oxide (F_{MnT})	Variable [c]
Highly reactive Mn oxide (F_{MnHR})	$F_{MnT} \times {}^1/_2$
Moderately reactive Mn oxide (F_{MnMR})	$F_{MnT} \times {}^1/_2$
Elemental sulfur (F_S)	0
Iron mono-sulfide (F_{FeS})	0
Pyrite (F_{FeS2})	0

[a] Zero flux (Neumann) conditions were prescribed for all variables at the lower boundary.
[b] Abbreviated to O_{2BW} in the main text.
[c] The flux of total manganese oxide was defined according to the bulk sedimentation rate assuming a 0.5 % Mn content (Glasby, 2006) in an analogous manner as described for Fe oxides in Table 2 (main text). This gives total fluxes of 187 and 30 μmol m^{-2} d^{-1} for shelf and slope settings, respectively, which are divided equally among Mn_{HR} and Mn_{MR}.

Table S1. Chemical species included in the model with corresponding boundary conditions at the sediment-water interface. Fixed seawater concentrations are defined for solutes (in mmol cm^{-3}) and constant fluxes to the seafloor for solids (in mmol cm^{-2} yr^{-1}).

Parameter	Equation
Porosity	$\varphi(z) = \varphi(L) + \big(\varphi(0) - \varphi(L)\big) \cdot \exp\left(-\dfrac{z}{z_{por}}\right)$
Diffusion coefficients	$D(z) = \dfrac{D_W}{1 - \ln(\varphi(z)^2)}$
Burial velocity of solids	$v_s(z) = \dfrac{\big(1 - \varphi(L)\big) \cdot \omega_{acc}}{\big(1 - \varphi(z)\big)}$
Burial velocity of solutes	$v_a(z) = \dfrac{\varphi(L) \cdot \omega_{acc}}{\varphi(z)}$
Bioturbation	$D_b(z) = D_b(0) \cdot \exp\left(-\dfrac{z^2}{2 \cdot z_{bt}^2}\right)$
Bioirrigation	$\alpha(z) = \alpha(0) \cdot \gamma \cdot \exp\left(-\dfrac{z}{z_{bio}}\right)$

Table S2. Depth–dependent constitutive equations used in the biogeochemical model.

Parameter	Description	Value	Unit	Source
L	Length of simulated sediment column	30	cm	1
S	Bottom water salinity	35	1	1
z_{dbl}	Diffusive boundary layer thickness	0.04	cm	2
ρ_s	Dry sediment density	2.5	g cm^{-3}	3
$\varphi(0)$	Porosity at 0 cm	0.9	1	1
$\varphi(L)$	Porosity at L cm	0.7	1	1
z_{por}	Porosity attenuation length	10	cm	1
z_{bt}	Bioturbation halving depth	3	cm	4
γ	Irrigation scaling coefficient for Fe^{2+}	0.2	1	5,9
γ	Irrigation scaling coefficient for other solutes	1	1	5
k_8	Rate constant for anaerobic oxidation of H$_2$S (DNRA)	0	M^{-1} yr^{-1}	1
k_9	Rate constant for anammox	1×10^8	M^{-1} yr^{-1}	6
k_{10}	Rate constant for aerobic oxidation of NH$_4^+$	1×10^7	M^{-1} yr^{-1}	6
k_{11}	Rate constant for aerobic oxidation of NO$_2^-$	1×10^7	M^{-1} yr^{-1}	6
k_{12}	Rate constant for aerobic oxidation of Mn^{2+}	5×10^6	M^{-1} yr^{-1}	3
k_{13}	Rate constant for aerobic oxidation of Fe^{2+}	5×10^8	M^{-1} yr^{-1}	3
k_{14}	Rate constant for anaerobic oxidation of Fe^{2+}	1×10^5	M^{-1} yr^{-1}	8
k_{15}	Rate constant for aerobic oxidation of H$_2$S	1×10^5	M^{-1} yr^{-1}	3
k_{16}	Rate constant for aerobic oxidation of FeS	1×10^5	M^{-1} yr^{-1}	3
k_{17}	Rate constant for aerobic oxidation of FeS$_2$	1×10^3	M^{-1} yr^{-1}	9
k_{18}	Rate constant for anaerobic oxidation of CH$_4$	1×10^5	yr^{-1}	10
k_{19}	Rate constant for FeS precipitation	1×10^6	M^{-1} yr^{-1}	9
k_{20}	Rate constant for FeS$_2$ precipitation	1×10^5	M^{-1} yr^{-1}	10
k_{21}	Rate constant for FeS$_2$ precipitation	1×10^5	M^{-1} yr^{-1}	10
k_{22}	Rate constant for H$_2$ oxidation	1×10^6	M^{-1} yr^{-1}	1
k_{23}	Rate constant for S^0 disproportionation	1	yr^{-1}	9
k_{24}	Rate constant for Mn$_{HR}$ / Mn$_{MR}$ reduction by Fe^{2+}	1×10^7 / 1×10^5	M^{-1} yr^{-1}	11
k_{25}	Rate constant for Mn$_{HR}$ / Mn$_{MR}$ reduction by H$_2$S	1×10^5 / 1×10^3	M^{-1} yr^{-1}	11
k_{26}	Rate constant for Fe$_{HR}$ / Fe$_{MR}$ / Fe$_{PR}$ / Fe$_U$ reduction by H$_2$S	100 / 0.1 / 3×10^{-4} / 0	M$^{-0.5}$ yr^{-1}	12
k_{27}	Rate constant for Mn$_{HR}$ ageing to Mn$_{MR}$	1.7	yr^{-1}	9
k_{28}	Rate constant for Fe$_{HR}$ ageing to Fe$_{MR}$	0.7	yr^{-1}	9
K_{O2}	Half–saturation constant for O$_2$ for OM degradation	1	μM	3
K_{NO3}	Half–saturation constant for NO$_3^-$ for OM degradation	10	μM	3
K_{NO2}	Half–saturation constant for NO$_2^-$ for OM degradation	10	μM	6
K_{Mn}	Half–saturation constant for Mn$_{HR}$ for OM degradation	0.1	wt–%	3
K_{Fe}	Half–saturation constant for Fe$_{HR}$ for OM degradation	0.6	wt–%	3
K_{SO4}	Half–saturation constant for SO$_4^{2-}$ for OM degradation	0.5	mM	3
r_{PC}	Atomic P-C ratio in deposited organic matter	1/106	mol P (mol C)$^{-1}$	13
r_{NC}	Atomic N-C ratio in deposited organic matter	16/106	mol P (mol C)$^{-1}$	13
a	Average lifetime of the reactive POC components	3×10^{-4}	yr	14
υ	Shape of gamma distribution for POC mineralization	0.125	1	14

Parameter values were based on the following sources: 1. This study. 2. Linke et al. (2005). 3. Van Cappellen and Wang (1996). 4. Boudreau (1997). 5. Meile et al. (2005), Dale et al (2013). 6. Bohlen et al. (2011). 7. Dale et al. (2012). 8. Dhakar and Burdige (1996). 9. Berg et al. (2003). 10. Dale et al. (2009). 11. Ref. 3 gives values of 10^6 and 10^4 for k_{24} and k_{25}, respectively, which correspond to the bulk mineral reactivity. Values for the HR and MR fractions arbitrarily increased and decreased from these values by a factor of 10, respectively. 12. Canfield et al. (1992) and Poulton et al. (2004). 13. Redfield et al. (1963). 14. Boudreau et al. (2008)

Table S3. Fixed model parameters. Variable parameters for shelf and slope settings are listed in Table 2 in the main text.

Rate	Stoichiometry	Footnote
	Organic matter mineralization reactions	a
R_1	$CN_{rNC}P_{rPC} + O_2 \rightarrow TCO_2 + r_{NC}NH_4^+ + r_{PC}PO_4^{3-}$	
R_2	$CN_{rNC}P_{rPC} + 2NO_3^- \rightarrow 2NO_2^- + TCO_2 + r_{NC}NH_4^+ + r_{PC}PO_4^{3-}$	
R_3	$CN_{rNC}P_{rPC} + 1.33NO_2^- \rightarrow 0.66N_2 + TCO_2 + r_{NC}NH_4^+ + r_{PC}PO_4^{3-}$	
R_4	$CN_{rNC}P_{rPC} + 2Mn_j \rightarrow 2Mn^{2+} + TCO_2 + r_{NC}NH_4^+ + r_{PC}PO_4^{3-}$	b
R_5	$CN_{rNC}P_{rPC} + 4Fe_j \rightarrow 4Fe^{2+} + TCO_2 + r_{NC}NH_4^+$	b
R_6	$CN_{rNC}P_{rPC} + 0.5SO_4^{2-} \rightarrow 0.5H_2S + TCO_2 + r_{NC}NH_4^+ + r_{PC}PO_4^{3-}$	
R_7	$CN_{rNC}P_{rPC} \rightarrow 0.5CH_4 + 0.5TCO_2 + r_{NC}NH_4^+ + r_{PC}PO_4^{3-}$	
	Secondary redox reactions	a
R_8	$H_2S + NO_3^-{}_{bac} \rightarrow SO_4^{2-} + NH_4^+$	
R_9	$NH_4^+ + NO_2^- \rightarrow N_2$	
R_{10}	$NH_4^+ + 1.5O_2 \rightarrow NO_2^-$	
R_{11}	$NO_2^- + 0.5O_2 \rightarrow NO_3^-$	
R_{12}	$Mn^{2+} + 0.5O_2 \rightarrow Mn_j$	b
R_{13}	$Fe^{2+} + 0.25O_2 \rightarrow Fe_j$	b
R_{14}	$Fe^{2+} + 0.2NO_3^- \rightarrow Fe_j + 0.1N_2$	b
R_{15}	$H_2S + 2O_2 \rightarrow SO_4^{2-}$	
R_{16}	$FeS + 2O_2 \rightarrow Fe^{2+} + SO_4^{2-}$	
R_{17}	$FeS_2 + 3.5O_2 \rightarrow Fe^{2+} + 2SO_4^{2-}$	
R_{18}	$CH_4 + SO_4^{2-} \rightarrow H_2S$	
R_{19}	$Fe^{2+} + H_2S \rightarrow FeS$	
R_{20}	$FeS + H_2S \rightarrow FeS + H_2$	
R_{21}	$FeS + S^0 \rightarrow FeS_2$	
R_{22}	$H_2 + EA \rightarrow ED$	c
R_{23}	$S^0 \rightarrow 0.25SO_4^{2-} + 0.75H_2S$	
R_{24}	$Mn_j + 2Fe^{2+} \rightarrow 2Fe_{HR} + Mn^{2+}$	d
R_{25}	$Mn_j + H_2S \rightarrow S^0 + Mn^{2+}$	d
R_{26}	$Fe_j + 0.5H_2S \rightarrow S^0 + Fe^{2+}$	e
R_{27}	$Mn_{HR} \rightarrow Mn_{MR}$	
R_{28}	$Fe_{HR} \rightarrow Fe_{MR}$	

[a] For clarity, H_2O is omitted from the reactions and they are not proton balanced. Particulate iron (Fe_j) and manganese oxides (Mn_j) are chemically defined as $Fe(OH)_3$ and MnO_2, respectively.
[b] For j = HR.
[c] Oxidation of H_2 is permitted by all electron acceptors, EA (O_2, NO_3^-, NO_2^-, Mn_{HR}, Fe_{HR} and SO_4^{2-}), leading to the formation of electron donors, ED (N_2, Mn^{2+}, Fe^{2+} and H_2S).
[d] For j = HR, MR.
[e] For j = HR, MR and PR.

Table S4. Reactions considered in the biogeochemical model.

Rate	Rate expression [a]	Unit [b]
R_1	$\sum_{i=1}^{14} k_i \cdot POC_i \cdot f_{K-O_2}$	mmol C cm^{-3} yr^{-1}
R_2	$\sum_{i=1}^{14} k_i \cdot POC_i \cdot \prod_{i=O_2,NO_2}(1 - f_{K-i})$	mmol C cm^{-3} yr^{-1}
R_3	$\sum_{i=1}^{14} k_i \cdot POC_i \cdot \prod_{i=O_2}(1 - f_{K-i})$	mmol C cm^{-3} yr^{-1}
R_4	$\sum_{i=1}^{14} k_i \cdot POC_i \cdot \prod_{i=O_2,NO_2,NO_3}(1 - f_{K-i})$	mmol C cm^{-3} yr^{-1}
R_5	$\sum_{i=1}^{14} k_i \cdot POC_i \cdot \prod_{i=O_2,NO_2,NO_3,Mn_{HR}}(1 - f_{K-i})$	mmol C cm^{-3} yr^{-1}
R_6	$\sum_{i=1}^{14} k_i \cdot POC_i \cdot \prod_{i=O_2,NO_2,NO_3,Mn_{HR},Fe_{HR}}(1 - f_{K-i})$	mmol C cm^{-3} yr^{-1}
R_7	$\sum_{i=1}^{14} k_i \cdot POC_i \cdot \prod_{i=O_2,NO_2,NO_3,Mn_{HR},Fe_{HR},SO_4}(1 - f_{K-i})$	mmol C cm^{-3} yr^{-1}
R_8	$k_8 \cdot NO_{3\ bac}^- \cdot H_2S$	mmol N cm^{-3} yr^{-1}
R_9	$k_9 \cdot NO_2^- \cdot NH_4^+$	mmol N$_2$ cm^{-3} yr^{-1}
R_{10}	$k_{10} \cdot O_2 \cdot NH_4^+$	mmol N cm^{-3} yr^{-1}
R_{11}	$k_{11} \cdot O_2 \cdot NO_2^-$	mmol N cm^{-3} yr^{-1}
R_{12}	$k_{12} \cdot O_2 \cdot Mn^{2+}$	mmol Mn cm^{-3} yr^{-1}
R_{13}	$k_{13} \cdot O_2 \cdot Fe^{2+}$	mmol Fe cm^{-3} yr^{-1}
R_{14}	$k_{14} \cdot NO_3^- \cdot Fe^{2+}$	mmol Fe cm^{-3} yr^{-1}
R_{15}	$k_{15} \cdot O_2 \cdot H_2S$	mmol S cm^{-3} yr^{-1}
R_{16}	$k_{16} \cdot O_2 \cdot FeS$	mmol Fe cm^{-3} yr^{-1}
R_{17}	$k_{17} \cdot O_2 \cdot FeS_2$	mmol Fe cm^{-3} yr^{-1}
R_{18}	$k_{18} \cdot CH_4 \cdot f_{SO4}$	mmol C cm^{-3} yr^{-1}
R_{19}	$k_{19} \cdot Fe^{2+} \cdot H_2S$	mmol Fe cm^{-3} yr^{-1}
R_{20}	$k_{20} \cdot FeS \cdot H_2S$	mmol Fe cm^{-3} yr^{-1}
R_{21}	$k_{21} \cdot FeS \cdot S^0$	mmol Fe cm^{-3} yr^{-1}
R_{22}	$k_{22} \cdot H_2 \cdot EA$	mmol EA cm^{-3} yr^{-1}
R_{23}	$k_{23} \cdot S^0$	mmol S cm^{-3} yr^{-1}
R_{24}	$k_{24-j} \cdot Mn_j \cdot Fe^{2+}$	mmol Mn cm^{-3} yr^{-1}
R_{25}	$k_{25-j} \cdot Mn_j \cdot H_2S$	mmol Mn cm^{-3} yr^{-1}
R_{26}	$k_{26-j} \cdot Fe_j \cdot H_2S^{0.5}$	mmol Fe cm^{-3} yr^{-1}
R_{27}	$k_{27} \cdot Mn_{HR}$	mmol Mn cm^{-3} yr^{-1}
R_{28}	$k_{286} \cdot Fe_{HR}$	mmol Fe cm^{-3} yr^{-1}

[a] Kinetic limiting terms: $f_{K-i} = \frac{[i]}{[i]+K_i}$, where K_i is the half–saturation constant for species i.

[b] Refers to cm^{-3} of pore fluid. The factor $f = \frac{100\ \% \cdot A_W \cdot \varphi(z)}{\frac{10^3 mmol}{mol} \cdot \rho_s \cdot (1-\varphi(z))}$ converts between wt % and mmol cm^{-3}, where A_W (g mol^{-1}) is the standard atomic weight of the element in question and ρ_s (2.5 g cm^{-3}) is the dry sediment density.

Table S5. Rate expressions and units.